



International Association
of Applied Mathematics and Mechanics
– Archive for Students –



From Problem to Failure – Insights from the Eigenvalue Problem of the Stiffness Matrix in Non-linear Structural Analysis

Chiara Hergl^{a,*} , Dominik Kern^b , Thomas Nagel^{b,c,d} 

^a Leibniz University Hannover, Institute of Applied Mathematics, Welfengarten 1, 30167 Hannover, Germany

^b Technische Universität Bergakademie Freiberg, Geotechnical Institute, Gustav-Zeuner-Str. 1, 09599 Freiberg, Germany

^c Freiberg Center for Water Research (ZeWaF), Freiberg, Germany

^d Helmholtz Centre for Environmental Research GmbH (UFZ), Department of Environmental Informatics, Germany

received 23.10.2024, accepted 03.02.2025, published 20.02.2025

* corresponding author: hergl@ifam.uni-hannover.de

Abstract: *Stiffness characterizes the response behaviour of systems and links generalized displacements and forces of that system. Stiffness matrices thus contain plenty of information about system behaviour. In a finite element setting, the global stiffness matrix is assembled and used in the analysis, but it is rarely output and subjected to analysis itself. Here, we use the eigendecomposition of the stiffness matrix in continuous and discrete mechanical settings. Particularly, we observe eigenvalues and eigenvectors in relation to structural failure in illustrative examples for educational purposes. Aside from the classical case of buckling modes, we study a particular strength reduction technique which is used in geotechnical engineering practice for ultimate limit state analyses. We briefly touch upon links to model reduction and check whether failure loads can be estimated from pre-failure information in non-linear settings. The paper has educational character, drawing links between different fields of engineering and emphasizing visualization.*

Keywords: stiffness matrix, singularity, limit states, material/geometrical non-linearity, failure, buckling

1 Introduction

Certain analysis procedures common in practice for establishing ultimate limit states (ULS) of structures proceed via a loss of convergence in implicit calculation schemes at the point where internal forces can no longer balance external forces. The point at which an iterative Newton-Raphson algorithm fails to obtain a solution to this force balance is dependent on time step size, non-linear tolerances, linear solver settings, mesh resolution, stress integration tolerances and other settings. Once the finite-element code exits with an error code, it remains to examine the last converged solution closely to assess whether the ULS was approached closely enough. Indications for such a failure are displacements approaching a pole or failure mechanisms traversing the entire structure in such a way that complete structural failure can be inferred.

There is, however, another way to look at this. Structural failure in the sense discussed here is linked to the stiffness matrix becoming singular. In other words, at

least one of its eigenvalues approaches zero. The associated eigenvector should then give clear indications of the failure mode. Simultaneously, the dominance of certain modes in the full displacement solution opens up avenues for model reduction, and thus simulations that are more efficient both in time and in terms of resources. The key to understanding and using this is the spectral decomposition or the eigenvalue problem known to all STEM graduates, for example from the determination of principal stresses and their directions. Although many textbooks on engineering mechanics contain a section on buckling, we refer to Bigoni [3] for further details on stability, as there are many illustrative examples. Similarly, stiffness matrices are covered in any textbook on Finite Elements sufficiently for our purpose; we recommend Hartmann [8], who takes a more general approach.

Following the educational purpose of the paper, we first illustrate this idea by a simple example from non-linear structural mechanics taught throughout basic engineering mechanics curricula, namely rod buckling. We then make the transition to a discrete setting where we examine the information content of the stiffness matrix in a linear finite element model and draw parallels to model reduction. Finally, we proceed to a non-linear ultimate limit state (ULS) analysis of slope failure using a strength-reduction technique prevalent in geotechnical engineering for assessing the safety of slopes, embankments, construction pits etc. There, we make use of both introductory examples to understand the results and re-iterate the model reduction link. We do so with minimum mathematical context aiming at a mix of formal and intuitive understanding by a combination of equations and visual illustration.

While our examples are all from the field of solid mechanics, the considerations are generalizable to other domains or coupled systems, such as poroelasticity, thermoelasticity or anything else with characteristics embedded in a system matrix / quasi-linear mapping. It is also worth noting that a singular stiffness matrix does not necessarily indicate failure, but also opens up new possibilities in the post-buckling period, such as vibration isolation [18] or functional mechanisms [15].

2 Definitions and hypothesis

We start with a stiffness matrix \mathbf{K} that depends on displacements \mathbf{u} , that is, $\mathbf{K}(\mathbf{u})$. This is because in linear problems with a constant stiffness matrix \mathbf{K} , nonlinear effects, such as stability loss and multivalent solutions, would be excluded. In practical terms, you need to make sure that nonlinear analysis is enabled in your simula-

tion software when you are going to analyze stability and safety of buckling-prone structures.

As customary, we condense external loading to a scalar load factor λ^F , which scales a prescribed load distribution. The variable λ is commonly used for eigenvalues and λ^F will be closely linked to this meaning in what follows, too. We further assume a stable unloaded initial state at $\lambda^F = 0$ and approach critical states by a load increase to a positive value $\lambda^F > 0$. When approaching a critical state, classical Newton-iterations in a quasi-static analysis fail to converge, since the stiffness matrix tends towards singularity, i.e. a vanishing stiffness in some sense. However, non-convergence is not a reliable indicator as it is sensitive to all kinds of numerical settings and could be related to other causes such as bad initial guesses or unsuitable load step sizes. Therefore, the actual cause for non-convergence needs to be identified. What we are looking for is an equilibrium state, in which there is (at least) one displacement direction without associated stiffness, implying failure of the structure¹. Mathematically, this corresponds to a nonlinear eigenvalue problem (EVP) of the form

$$\mathbf{K}(\mathbf{u}(\lambda^F))\mathbf{v}^F = \mathbf{0} \quad \text{with} \quad \mathbf{K}(\mathbf{u}(\lambda^F))\mathbf{u}(\lambda^F) = \mathbf{f}(\lambda^F). \quad (1)$$

Its eigenvalues λ_i^F are the critical loads that make the stiffness matrix singular. In terms of mathematics, a singular stiffness matrix indicates a bifurcation. On crossing bifurcation points, solutions change stability and start or cease to exist. For a detailed discussion of bifurcations we refer to general system theory [7]. In most cases, the lowest critical load is relevant for design, but we keep in mind, that the corresponding failure mechanisms, indicated by the eigenvectors \mathbf{v}_i^F , may change depending on properties and constraints of the system. In other words, boundary conditions may stabilize one failure mode and destabilize another, such that a failure mechanism initially corresponding to a higher load may become associated with the lowest critical load.

We remember that $\mathbf{u}(\lambda^F)$ is a one-to-many relation, at the latest after the first bifurcation of the solution, and therefore so is $\mathbf{K}(\mathbf{u}(\lambda^F))$. Strictly speaking, we should denote the eigenvalues λ_i^F by referring to a solution branch. For sake of simplicity, we assume that the initial unbuckled state remains, even when it becomes mechanically unstable.

Our idea to evaluate the ordinary EVP of \mathbf{K} for failure estimation is motivated by observations we made in numerical simulations and the convenience that the stiffness matrix comes for free in typical analysis types,

¹You can think of a horizontal force-displacement curve, where at a given force, the displacement can grow without bounds.

as it is computed anyway. The ordinary eigenvalues λ_i of the stiffness matrix \mathbf{K} correspond to the stiffnesses in the directions of the associated eigenvectors $\mathbf{v}_i \neq \mathbf{0}$, which is obvious, when we write the EVP like that

$$\mathbf{K}(\mathbf{u}(\lambda^F))\mathbf{v} = \lambda\mathbf{v}. \quad (2)$$

The ordinary eigenvector \mathbf{v}_0 corresponding to the lowest ordinary eigenvalue λ_0 of the stiffness matrix $\mathbf{K}(\mathbf{u}(\lambda^F))$ coincides with the eigenvector \mathbf{v}_i^F of the nonlinear EVP (1), because at critical loads $\lambda^F = \lambda_i^F$ the stiffness matrix gets singular, i.e. $\det(\mathbf{K}(\mathbf{u}(\lambda_i^F))) = 0$. Since the determinant is the product of the eigenvalues $\det(\mathbf{K}(\mathbf{u}(\lambda_i^F))) = \lambda_0\lambda_1\lambda_2\dots$ the lowest² ordinary eigenvalue must be zero $\lambda_0 = 0$. On rearranging the ordinary EVP (2) slightly differently

$$(\mathbf{K}(\mathbf{u}(\lambda^F)) - \lambda\mathbf{I})\mathbf{v} = \mathbf{0}. \quad (3)$$

and setting $\lambda = \lambda_0 = 0$, we have the same equation defining the eigenvectors as in the nonlinear EVP (1).

So far everything is well known. To proceed further we hypothesize that the eigenvector \mathbf{v}_0 of the stiffness matrix corresponding to the lowest eigenvalue provides a useful estimator for the failure mode already before we reach failure. This would be useful for numerical analyses that stop converging some time before one of the eigenvalues reaches zero. We use the notation $\mathbf{v}_i(\lambda^F)$ to indicate that we compute the eigenvectors of the stiffness matrix at the given load λ^F . In such simulations we found evidence that the eigenvector $\mathbf{v}_0(\lambda^F < \lambda_0^F)$ predicts upcoming failure quite well, i.e. $\mathbf{v}_0(\lambda^F < \lambda_0^F) \sim \mathbf{v}_0(\lambda_0^F)$ with λ_0^F denoting the lowest critical load and $\lambda_0 = 0$ the vanishing stiffness in the direction of \mathbf{v}_0 . By assumption, the load factor λ^F is positive and so are the nonlinear eigenvalues $\lambda_i^F > 0$. The eigenvalues of the ordinary EVP may become negative indicating that the load exceeds a critical load, e.g. when we would evaluate the eigenvalues of $\mathbf{K}(\lambda_1^F)$ then we were beyond the lowest critical load $\lambda_1^F > \lambda_0^F$ and have one negative eigenvalue λ_i .

3 Basic examples

In the first example, a variation of the well-known Euler buckling, we estimate buckling loads and mode shapes. After discretization we have a stiffness matrix to compute eigenvalues/-vectors, and test our hypothesis. In the second example we subject a rod simply to tensile

²By low we refer to the absolute value, further we assume the eigenvalue/-vector pairs to be sorted by the absolute value of the eigenvalue in ascending order.

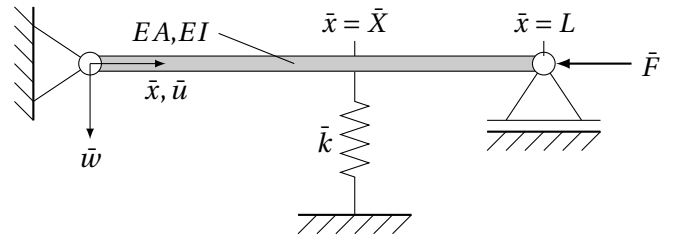


Figure 1 – An axially loaded rod hinged at both ends with a stabilizing lateral spring at \bar{X} .

loading along its axis in a linear analysis but transition to a finite-element setting. No instability occurs in this second case. Instead, we illustrate the interpretation of the eigenvectors of the stiffness matrix in the context of boundary conditions and reveal their potential use in model reduction.

3.1 Rod buckling

Rod buckling exhibits the characteristic features of stability problems. Failure means in this context a vanishing stiffness in axial direction, when the rod bends in transversal direction, either left or right in a two dimensional setting. It is a simple, illustrative example and after discretization based on a kinematic Ansatz leads to an equation system

$$\mathbf{K}(\mathbf{u})\mathbf{u} = \mathbf{f}, \quad (4)$$

which is a common sight in numerical mechanics, such as when using the finite element method (FEM).

3.1.1 Physical model

Our example, shown in Figure 1, corresponds to the second Euler case extended by a stabilizing spring added somewhere along the rod. The elastic potential for a rod with coupled bending and axial displacements (length L , Young's Modulus E , cross section area A , area moment of inertia or second moment of area I), a discrete spring (stiffness \bar{k}) and a conservative load (force \bar{F}) reads [19]

$$\bar{\Pi} = \frac{1}{2} \int_0^L \left[EI \bar{w}''(\bar{x})^2 + EA \left(\bar{u}' + \frac{1}{2} \bar{w}'^2 \right)^2 \right] d\bar{x} + \frac{1}{2} \bar{k} \bar{w}(\bar{X})^2 + \bar{F} \bar{u}(L). \quad (5)$$

For the sake of simplicity, we assume constant cross-sectional parameters $EI = \text{const.}$ and $EA = \text{const.}$ On non-dimensionalization [11] with reference length L and reference force $\frac{EI}{L^2}$, i.e. $x = \frac{\bar{x}}{L}$, $X = \frac{\bar{X}}{L}$, $u = \frac{\bar{u}}{L}$, $w = \frac{\bar{w}}{L}$

and $\Pi = \frac{\bar{\Pi}L}{EI}$, we obtain the non-dimensional potential

$$\Pi = \frac{1}{2} \int_0^1 \left[w''(x)^2 + G \left(u' + \frac{1}{2} w'^2 \right)^2 \right] dx + \frac{1}{2} k w(X)^2 + Fu(1), \quad (6)$$

with the non-dimensional parameters: squared slenderness ratio, non-dimensional spring stiffness and non-dimensional load, respectively, given by

$$G = \frac{AL^2}{I}, \quad (7a)$$

$$k = \frac{\bar{k}L^3}{EI}, \quad (7b)$$

$$F = \frac{\bar{F}L^2}{EI}. \quad (7c)$$

The buckling loads for a simple rod without spring ($k = 0$), also referred to as Euler's critical loads, are $F_i = (i\pi)^2$ with $i = 1, 2, 3, \dots$

Let's come back to the kinematic Ansatz mentioned earlier. We apply Ritz's method [19] approximating the axial displacement by a linear function, which is exact for the case of pure compression, and two sinusoidal modes for the transversal displacement (bending)

$$u \approx \hat{u}x, \quad (8a)$$

$$w(x) \approx \sum_{j=1}^2 \hat{w}_j \sin(j\pi x). \quad (8b)$$

We use two modes for bending, because we want to find out how the buckling mode shapes depend on the properties of the spring (stiffness k , position X).

Application of Ritz's method leaves us with three degrees of freedom, sometimes called Ansatz free values, which we collect in a generalized displacement vector $\mathbf{u} = [\hat{w}_1, \hat{w}_2, \hat{u}]^T$. We expect two buckling modes to which we refer to as *lower* and *higher* for the respective buckling load to distinguish them from the basis indexed by numbers (w_1, w_2) given in (8b). This two-mode Ansatz may seem limited, however, it reflects the fact that often we are practically interested in the lowest mode only (upcoming failure) and some outlook beyond it. By outlook we mean to check, whether a small change in boundary conditions or loading may allow one of the higher modes to become the lowest.

The next steps are straightforward: we differentiate the potential (6) twice with respect to our degrees-of-freedom to obtain the stiffness matrix

$$\mathbf{K} = \frac{\partial^2 \Pi}{\partial \mathbf{u}^2} \quad (9)$$

Table 1 – Parameter values of the quantitative example (non-dimensional).

G	100 ²	squared slenderness ratio
X	$\begin{cases} 0.50 \\ 0.55 \end{cases}$	centre position off-centre position
k	0...300	spring stiffness

with

$$K_{11} = \frac{9\pi^4 G \hat{w}_1^2}{16} + \frac{3\pi^4 G \hat{w}_2^2}{2} + \frac{\pi^2 G \hat{u}}{2} + \frac{\pi^4}{2} + k \sin(\pi X), \quad (10a)$$

$$K_{12} = K_{21} = 3\pi^4 G \hat{w}_1 \hat{w}_2 + k \sin(\pi X) \sin(2\pi X), \quad (10b)$$

$$K_{13} = K_{31} = \frac{\pi^2 G \hat{w}_1}{2}, \quad (10c)$$

$$K_{22} = \frac{3\pi^4 G \hat{w}_1^2}{2} + 9\pi^4 G \hat{w}_2^2 + 2\pi^2 G \hat{u} + 8\pi^4 \quad (10d)$$

$$+ 2k \sin(\pi X) \sin(2\pi X) \cos(\pi X), \quad (10e)$$

$$K_{23} = K_{32} = 2\pi^2 G \hat{w}_2, \quad (10f)$$

$$K_{33} = G. \quad (10g)$$

Remember that the degrees-of-freedom depend on the load factor by the equilibrium condition of the nonlinear EVP (1), which means $\hat{w}_1(\lambda^F)$, $\hat{w}_2(\lambda^F)$ and $\hat{u}(\lambda^F)$ in our example. Since we assume loading by the axial force only

$$\mathbf{f}(\lambda^F) = \lambda^F \begin{bmatrix} 0 \\ 0 \\ F = 1 \end{bmatrix}, \quad (11)$$

there is no bending ($w_1 = w_2 = 0$) in the pre-buckled state, which simplifies the stiffness matrix \mathbf{K} . For further details we refer to the supplementary material.

3.1.2 Quantitative example

We choose a slender rod with a spring positioned in its centre or close by. Its numerical values are listed in Table 1.

Let's start with the buckling loads. We compute them from the nonlinear EVP (1) and plot them in Figure 2. Let's first interpret the results for the spring in the centre position. The sloped line, independent of its color, corresponds to the buckling mode shape coinciding with w_1 , and is given by the linear function $F_1 = \frac{k}{\pi^2} + \pi^2$. Similarly, the horizontal line $F_2 = 4\pi^2$ corresponds to mode shape w_2 . At a spring stiffness $k_{\text{cross}} = \frac{3}{2}\pi^4 \approx 146.11$ the buckling load is the same for both modes, i.e. there is not a single mode shape but a manifold of mode shapes, since linear combinations of w_1 and w_2 may occur in addition to the two modes themselves. Mathematically, we have

a bifurcation of co-dimension two that is characterized by a zero eigenvalue of multiplicity two [10]. The physical interpretation behind these calculations is that the central spring stabilizes only the w_1 mode, whereas it is ineffective for the w_2 mode which by definition (8b) has a node in the rod's center. The colors of the lines in Figure 2 show which of the buckling loads is the lower (blue) and which is higher (red) one. For the central spring, the blue line for the lower buckling mode matches exactly the w_1 basis in the lower range $0 \leq k < k_{\text{cross}}$ and the w_2 basis in the higher range $k_{\text{cross}} \leq k < \infty$, and vice versa for the red line of the higher mode. The message to remember is that the buckling mode shape (lower, higher) depends on system properties or constraints, here represented by the spring, and may change.

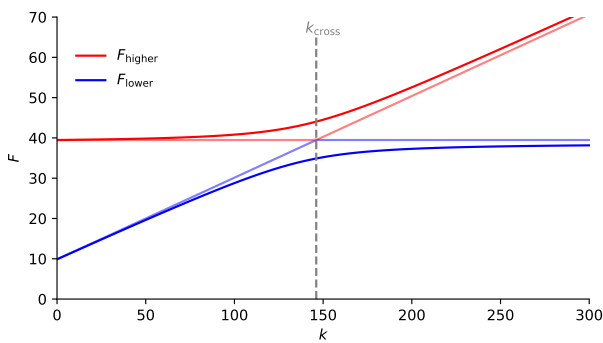


Figure 2 – Buckling loads versus spring stiffness with spring at centre (semi-transparent straight lines) and off-centre position (fully opaque curved lines).

From the fully opaque lines in Figure 2 we find the buckling loads of the off-centre case being smoothed versions of the centre-case. There is no longer any sharp transition as seen with the central spring, since the spring now couples effectively both basis shapes w_1 and w_2 .

Consequently, the buckling mode shapes are now linear combinations of both Ansatz functions with a mode's dominance depending on spring stiffness. To reveal what the buckling modes look like and how their transition proceeds, we plot the buckling mode shapes for varying spring stiffness in Figure 3. The notion of *low* and *high* stiffness is to be understood in relation to the crossing point k_{cross} . With the spring in the off-centre position the mode switch occurs at $k_{\text{cross}} \approx 153.65$, if we define $\hat{w}_1 = \hat{w}_2 = \frac{\sqrt{2}}{2}$ as the crossing condition (normalized eigenvectors $\|v_i^F\| = 1$ with $\hat{u} = 0$). For a low spring stiffness, we observe buckling mode shapes similar to classical rod buckling ($k = 0$), they correspond to mode shapes close to w_1 . Whereas mode shapes associated with the higher load are close to w_2 . For the intermediate spring stiffness, lower and higher buckling

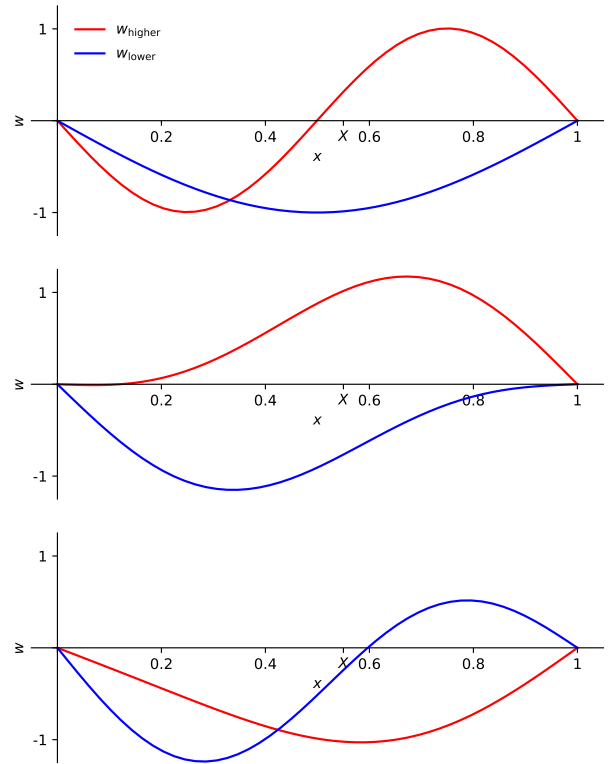


Figure 3 – Buckling mode shapes in the off-centre case for three values of the spring stiffness (from top to bottom): low $k = 3$, intermediate $k = 150$ and high $k = 300$. Spring position marked by X .

mode are almost symmetric with respect to the rod's centre (for $X = 0.5$ and $k = k_{\text{cross}}(X = 0.5)$ they would be exactly symmetric). One can observe how the lower mode is shifting due to the constraint imposed by the spring. For a high spring stiffness, we observe a swap in the sense that now the lower buckling load causes a mode shape close to w_2 and the higher one close to w_1 . The constraining effect of the spring now becomes quite apparent. The transition from top to bottom, as k increases, is smooth in the mode shapes, whereas for the spring in central position the mode shapes remain constant and at $k = k_{\text{cross}}$ there is a sudden take-over in the buckling loads. Note in passing, that this observed mode swap resembles frequency veering in vibrational systems [13] and points to interesting parallels between vibrations and stability [17].

Now let's test our hypothesis and evaluate the ordinary EVP for sub-critical loads $0 < F < F_{\text{lower}}$ and estimate the buckling mode shapes. In Figure 4 we plot the composition of the lower buckling mode shape in terms of the degrees-of-freedom of each basis function and find an increasing match of the estimator for $F < F_{\text{lower}}$. In accordance with Equation (3) the match is perfect for $F = F_{\text{lower}}$. Similarly, we plot our estimator for the higher

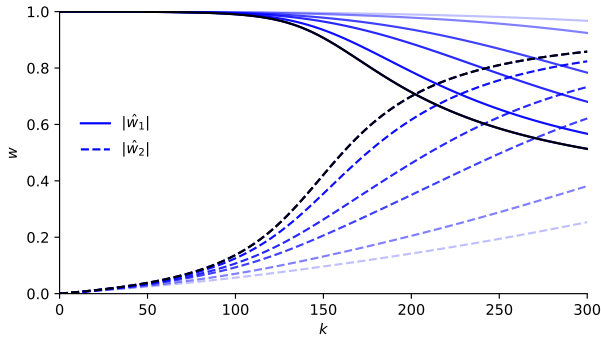


Figure 4 – Mode shape estimation for the lower buckling load computed at $F/F_{\text{lower}} = \{0.25, 0.5, 0.75, 0.85, 0.95, 1.0\}$ with increasing opacity (blue). The lines for $F = F_{\text{lower}}$ coincide with the exact values (black). The zero component $\hat{u} = 0$ is not shown.

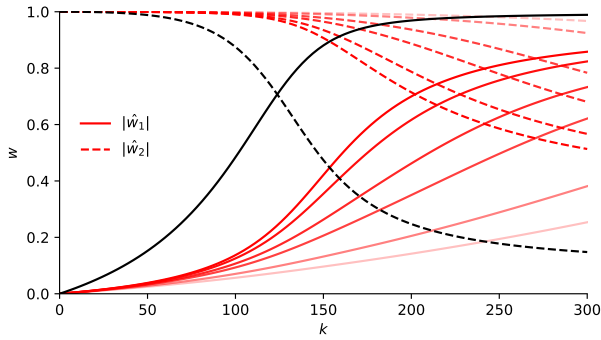


Figure 5 – Mode shape estimation for the higher buckling load computed at $F/F_{\text{lower}} = \{0.25, 0.5, 0.75, 0.85, 0.95, 1.0\}$ with increasing opacity (red). The exact values (black) were obtained for $F = F_{\text{higher}}$, which may be unreachable in practical simulations due to failure at F_{lower} . The zero component $\hat{u} = 0$ is not shown.

buckling mode shape in Figure 5 and again observe an increasingly better match with increasing load F , not getting the perfect match, since $F_{\text{lower}} < F_{\text{higher}}$.

Finally, we check the possibility to extrapolate the eigenvalues, particularly the lowest, as function³ of the load $\lambda_0(\lambda^F)$. From Figure 6 we find that the lowest eigenvalue varies almost linearly with the load in our example. The kinks in this plot are either due to absolute value or to the next eigenvalue taking over the minimum. We sort the eigenvalues by absolute value and so we did the plots, that you can read off the crossings. Their signs are all positive in the unloaded state $\lambda_i(\lambda^F = 0) > 0$ and become negative after their corresponding critical load. A

³To make this function univalent, we assume that the rod remains in the unbuckled state, even when it is (mechanically) instable.

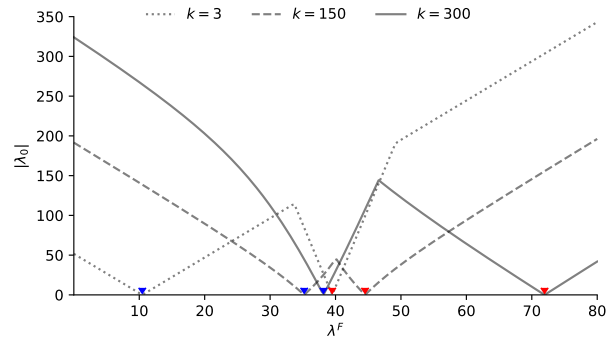


Figure 6 – Lowest eigenvalue by absolute value during loading for three different values of the spring. The blue and red ticks mark lower and higher buckling loads, respectively.

negative sign then indicates how far the current load exceeds the critical load while the next critical load (higher mode) comes closer to zero and takes over the lowest absolute value. Thus, we have good conditions for linear extrapolation of the eigenvalues' zero-crossing. In other words, loads at failure can be estimated based on pre-failure information. Of course one specific example is not sufficient, but it renders further study worthwhile. We will get back to this in the ultimate limit state example in Section 4.

3.2 Finite element stiffness matrix – discrete model

Before coming to the application example of a non-linear FE analysis for ultimate limit state analyses, we examine the stiffness matrix resulting from a simple one-dimensional linear finite element analysis of a rod under tensile loading. The intent here is to provide a simple example for the interpretation and use of the eigen-decomposition of a FE stiffness matrix in a linear case without instability with a pointer towards model-order reduction.

3.2.1 Discrete model

Consider a rod of length L which we discretize into finite elements of equal length h . The resulting stiffness matrix of the linear system $\mathbf{Ku} = \mathbf{f}$ reads in case of spatially uniform tensile stiffness EA and separation into four finite elements of length $h = L/4$ with five nodes

$$\mathbf{K} = 4 \begin{bmatrix} 1 & -1 & 0 & 0 & 0 \\ -1 & 2 & -1 & 0 & 0 \\ 0 & -1 & 2 & -1 & 0 \\ 0 & 0 & -1 & 2 & -1 \\ 0 & 0 & 0 & -1 & 1 \end{bmatrix} \quad (12)$$

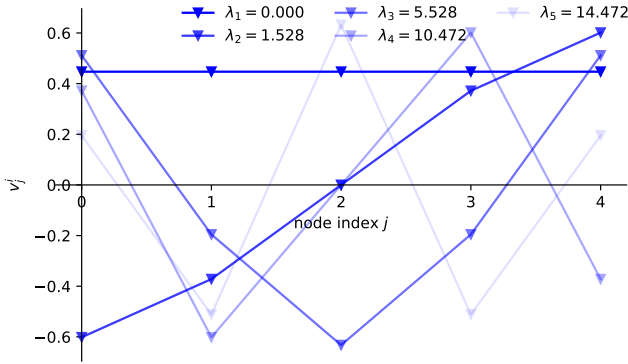


Figure 7 – Eigenvalues and -vectors for the stiffness matrix of the free rod from Eq. (12). The sequence of modes can be recognized by decreasing opacity and wavelength.

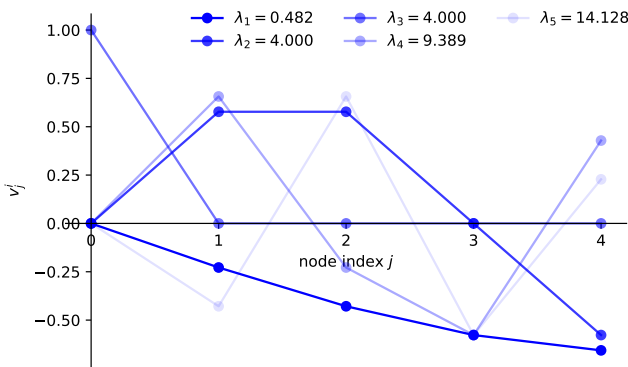


Figure 8 – Eigenvalues and -vectors for the stiffness matrix of the constrained rod from Eq. (13). The sequence of modes can be recognized by decreasing opacity and wavelength.

For the above, we normalized forces and displacements, \mathbf{f}/EA and \mathbf{u}/L , to obtain non-dimensional stiffness matrices as in the previous example. The factor four comes from the above mentioned discretization $L/h = 4$. Eigenvalues and eigenvectors of this stiffness matrix are shown in Figure 7 for the case without boundary conditions, Eq. (12), and in Figure 8 for the case with boundary conditions, Eq. (13). In both figures, v_j^i indicates the value of the j^{th} coordinate of the eigenvector associated with the i^{th} eigenvalue λ_i .

We observe in Figure 7 that the lowest eigenvalue with vanishing stiffness corresponds to a rigid body mode⁴, while the spatial frequency of the eigenmodes increases with the associated stiffness, until we have alternating compression and expansion in each of the finite elements for the highest eigenvalue.

To eliminate the rigid body mode, we constrain node zero with a no-displacement boundary condition, chang-

⁴This lack of constraint could also be interpreted as a structural failure, as the structure has no bearing to react against.

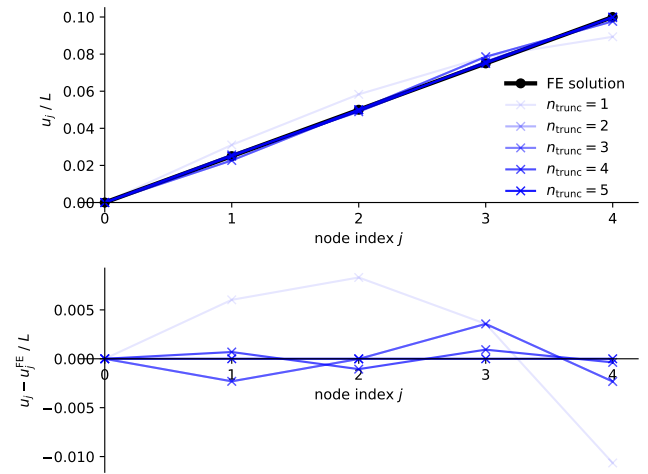


Figure 9 – FE solution and its reconstruction by summing up modes using Eq. (14) (top). Bottom figure shows deviation from exact solution. Opacity increases with the highest mode considered in the summation.

ing the stiffness matrix to

$$\mathbf{K} = 4 \begin{bmatrix} 1 & 0 & 0 & 0 & 0 \\ 0 & 2 & -1 & 0 & 0 \\ 0 & -1 & 2 & -1 & 0 \\ 0 & 0 & -1 & 2 & -1 \\ 0 & 0 & 0 & -1 & 1 \end{bmatrix} \quad (13)$$

The corresponding spectral decomposition yields a strictly positive lowest eigenvalue and a corresponding deformation mode that corresponds to a spatially monotonic displacement, cf. Figure 8. We also observe that all eigenmodes satisfy the boundary condition at node 0, except for one. This one will map the reaction force at the Dirichlet boundary.

We now solve the system with a non-dimensional external load of 0.1 on node 5 obtaining the FE solution in Figure 9. For a further interpretation of the eigenvectors, we look at the spectral decomposition $\mathbf{K} = \mathbf{\Lambda}\mathbf{V}\mathbf{V}^{-1}$ with $\mathbf{\Lambda} = \text{diag}(\lambda_i)$. This allows us to diagonalize the linear system to

$$\mathbf{\Lambda} \underbrace{(\mathbf{V}^{-1}\mathbf{u})}_{\tilde{\mathbf{u}}} = \underbrace{\mathbf{V}^{-1}\mathbf{f}}_{\tilde{\mathbf{f}}} \quad (14)$$

This allows us to draw links to model order reduction by truncating the modes used in $\mathbf{\Lambda}$ (diagonal matrix containing the eigenvalues) and \mathbf{V} (matrix containing the eigenvectors) in Eq. (14) at a certain number. Alternatively, we can write this as

$$\mathbf{u}^{\text{FE}} \approx \sum_{i=1}^{n_{\text{trunc}}} \lambda_i^{-1} (\mathbf{v}^i \cdot \mathbf{F}) \mathbf{v}^i \quad (15)$$

In other words, the solution space is spanned by the eigenvectors. Each solution contribution in the sum is co-linear with its basis/eigenvector and scaled by the load vector projected onto that basis divided by the associated stiffness. The result of truncating the sum at different orders is shown in Figure 9.

We observe that the linear displacement (constant strain) profile in the rod is recovered precisely if all modes are included, while increasing deviations occur with earlier truncation. Arguably, already the base mode constitutes a reasonably good approximation of the solution. We see in Equation (15), that each mode is weighted by the inverse of the eigenvalue. In other words, the smaller an eigenvalue is in relation to the others, the more its associated deformation mode will contribute to the overall solution. This, and the particular relevance of the lowest eigenmode explained in the example of buckling, motivates further the study of the lowest eigenmode in the non-linear FE problem of the next section.

4 Strength reduction – global limit state

The findings are now transferred to a non-linear FE model. For this purpose, we will look at a slope failure simulation typical in geotechnical engineering. We will investigate the meaning of the eigenvector corresponding to the lowest eigenvalue in light of the model reduction idea as well as the trends of the eigenvalues in light of our hypothesis.

In a non-linear FE analysis we solve for a vanishing residual vector \mathbf{R} given by the difference between internal and external forces, sometimes called out-of-balance forces, $\mathbf{R} = \mathbf{F}_{\text{int}} - \mathbf{F}_{\text{ext}}$. When the external forces are incremented in a load or time step, the corresponding displacement increment $\Delta\mathbf{u}$ is sought iteratively. A Newton-Raphson linearization gives rise to the following linear system solved in each iteration of each load increment:

$$\mathbf{K}(\mathbf{u})\Delta\Delta\mathbf{u} = -\mathbf{R} \quad (16)$$

Here, $\Delta\Delta\mathbf{u}$ is the Newton update for the sought displacement increment $\Delta\mathbf{u}$. The stiffness matrix constitutes the tangent of the problem in the sense of $\mathbf{K} = \partial\mathbf{R}/\partial\Delta\mathbf{u}$.

4.1 Example: strength reduction in geotechnical engineering

Pressure-dependent strength of granular materials is often described in terms of limit states defined based on

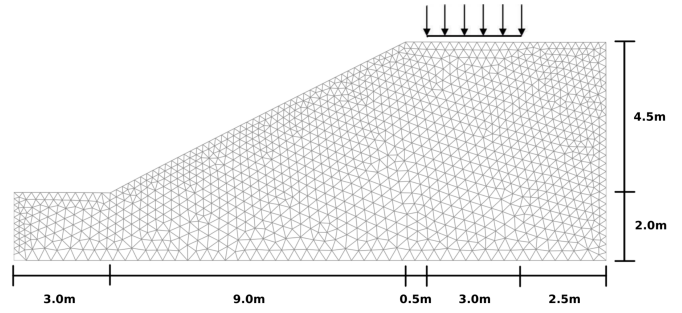


Figure 10 – Slope failure analysis: A load of 30 kPa is applied to the top of the slope over an area of 3 m in length. The bottom is fixed in all directions, the sides are constrained horizontally.

Coulomb's or Mohr-Coulomb's law, respectively⁵:

$$\tau \leq c + \sigma'_n \tan \varphi \quad (17)$$

$$\frac{\sigma_1 - \sigma_3}{2} \leq \frac{\sigma'_1 + \sigma'_3}{2} \sin \varphi + c \cos \varphi \quad (18)$$

The material parameters cohesion c and internal friction angle φ are at the basis of the associated strength reduction techniques. These so-called φ - c reduction methods have become popular due to their easy integration into standard displacement-based finite element approaches and were compared to actual limit state analyses based on the upper and lower bounds established under certain assumptions by plasticity theory [5, 16]. They can be extended towards less restrictive assumptions, e.g. non-associated flow rules [16], complex geotechnical settings and structures [2], as well as coupled problems [9]. The objective of the analysis is to determine a safety factor F with respect to the ultimate limit state by slowly reducing the strength parameters of a soil, namely the angle of internal friction φ and the cohesion c in a Mohr-Coulomb strength model, until structural failure is reached.

Instead of increasing the external loads, a reduction coefficient η_{trial} is increased over (pseudo-)time to produce a set of reduced strength parameters c_{trial} and φ_{trial} following the so-called Fellenius rule, i.e.

$$c_{\text{trial}} = \frac{c}{\eta_{\text{trial}}}, \quad (19a)$$

$$\varphi_{\text{trial}} = \arctan\left(\frac{\tan \varphi}{\eta_{\text{trial}}}\right). \quad (19b)$$

η_{trial} is a scalar parameter with a similar role to the load factor λ^F . Instead of increasing the load, η_{trial} scales down the strength. This reduction continues until no

⁵Here, a soil mechanical sign convention is used in which compressive stresses are positive. The prime indicates effective stresses.

static equilibrium can be achieved. In other words, the internal forces can no longer balance the external loads and the slope fails. Practically, the Newton-Raphson equilibrium iterations no longer converge at some stage at which state one determines the safety factor from the last trial value, $\eta = \eta_{\text{trial, last}}$.

To make sure that structural failure occurred and the nonlinear analysis did not fail for other reasons, the analyst verifies the ultimate limit state by looking at poles in the displacement solution and equivalent plastic strain bands traversing the structure. Here, we additionally analyse the global stiffness matrix of the finite element analysis in the last converged load step.

4.2 Model

The slope analysis example, shown in Figure 10, was motivated by an example realized in PLAXIS2D [14] and also implemented in OpenGeoSys [4]. A smoothed version of the Mohr-Coulomb material model was used [1, 12].

The specific simulation settings are not relevant here but can be found in [6]. A distributed load is applied on top of a slope as indicated in Figure 10. The simulation starts by applying gravity and top load gradually in the first 2 s of the simulation⁶. After a hold phase of 1 s, strength reduction commences as indicated in Table 2.

In the base case, slope failure is reached after $t = 5.375$ s. The base case uses the numerical settings indicated in [6] and linear triangular elements.

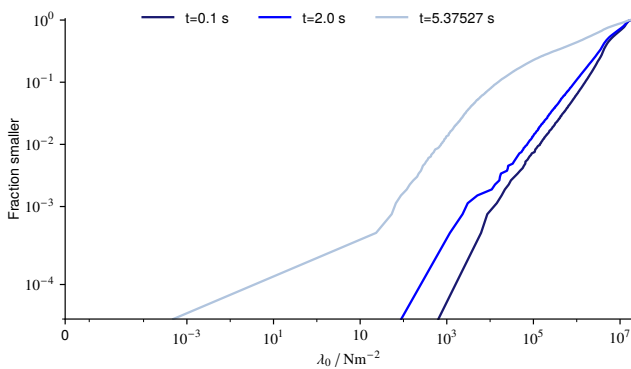


Figure 11 – Cumulative distribution function of eigenvalues of the global stiffness matrix at different time points of the simulation (base case TRI3a).

⁶Note, that a quasi-static analysis is used and the material model is rate-independent. Therefore, time here is just a pseudo time used to advance loading and strength reduction. Time steps therefore constitute load steps.

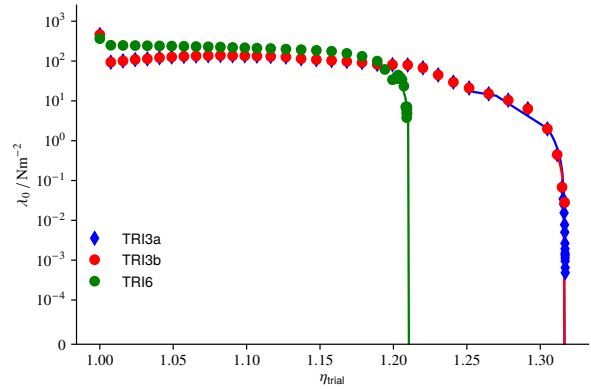


Figure 12 – Extrapolation of the eigenvalue λ_0 as a function of the reduction coefficient.

4.3 Analyzing the global stiffness matrix

For the analysis of the finite element stiffness matrix, we will look at three different load steps with the following time stamps:

- $t = 0.1$ s, i.e. at the beginning of the simulation when the material is still elastic,
- $t = 2.0$ s after full loading has been reached, and
- $t = 5.375$ s, i.e. the last converged load step before failure.

The cumulative distribution function of the eigenvalues of the global stiffness matrix at these load steps is shown in Figure 11. One can observe a range of well-defined positive values in the elastic structure indicated by the blue curve. After load application, some plasticity already occurred, shifting the curve to the left (green) but maintaining a sound load-bearing structure. At the end of strength reduction (red) the curve has shifted to much lower stiffness values due to increasing plastification of the slope. The formation of a continuous shear band causes structural failure which is nicely demonstrated in Figure 11 by the global stiffness matrix becoming singular (lowest eigenvalue very close to zero).

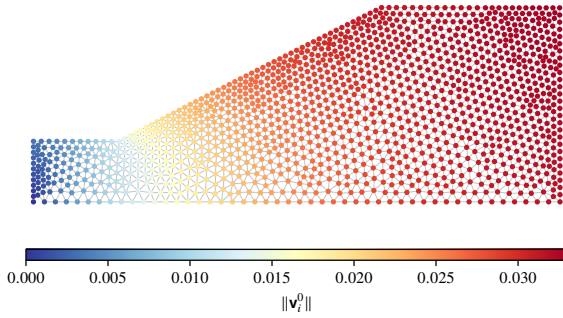
As in the buckling load example, the evolution of the eigenvalues is analyzed, cf. Figure 12. In contrast to the introductory example, where the eigenvalue is analyzed as a function of the load factor λ^F , the eigenvalue is analyzed as a function of the reduction coefficient η_{trial} reducing material strength. We observe towards the end of the base case (TRI3a) simulation a rapidly increasing rate at which the lowest eigenvalue λ_0 decreases. The extrapolated zero value of $\eta_{\text{trial}} = 1.317$ indicates the reduction coefficient at which the slope fails, i.e. the factor of safety determined in the calculation.

We compared the base case (TRI3a) with two other simulation settings in Fig. 12. One simulation (TRI3b)

		0 s	1 s	2 s	3 s	4 s	5 s	6 s	7 s
Density	$\rho / \text{kg m}^{-3}$	0	1600	1600	1600	1600	1600	1600	1600
Top loading	$p_{\text{top}} / \text{kPa}$	0	15	30	30	30	30	30	30
Cohesion	c / kPa	1	1	5	5	4.5	4	3.5	3
Friction angle	$\varphi / ^\circ$	20	20	20	20	18.12	16.24	15.26	12.32
Safety factor	η_{trial}	1	1	1	1	1.11111	1.25	1.42871	1.66667

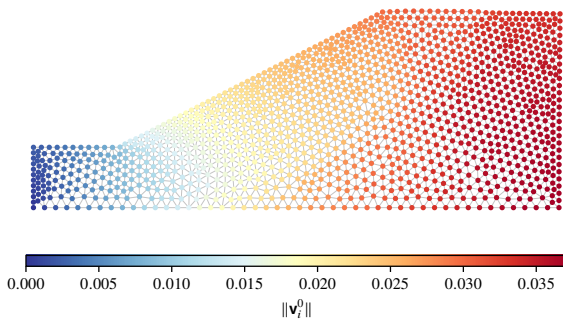
Table 2 – Parameter values for slope failure analysis. In the first two seconds, gravity and external load are being linearly ramped up. The actual strength reduction commences after 3 s.

$$\lambda^0 = 639.8957 \text{ Nm}^{-2}$$



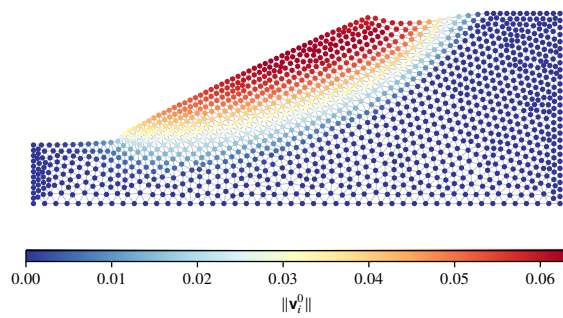
(a) Slope $t = 0.1 \text{ s}$

$$\lambda^0 = 476.1906 \text{ Nm}^{-2}$$



(b) Slope $t = 2.0 \text{ s}$

$$\lambda^0 = 0.0005 \text{ Nm}^{-2}$$

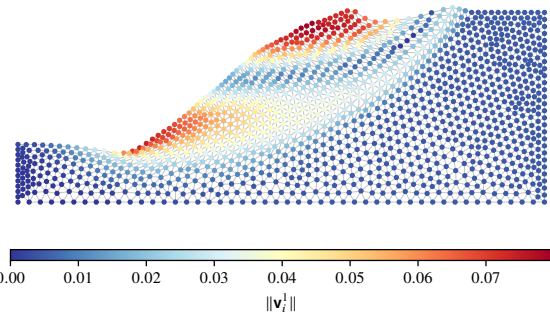


(c) Slope $t = 5.375 \text{ s}$

Figure 13 – Eigenvector analysis corresponding to the smallest eigenvalue at different load steps. Plot over deformed configuration.

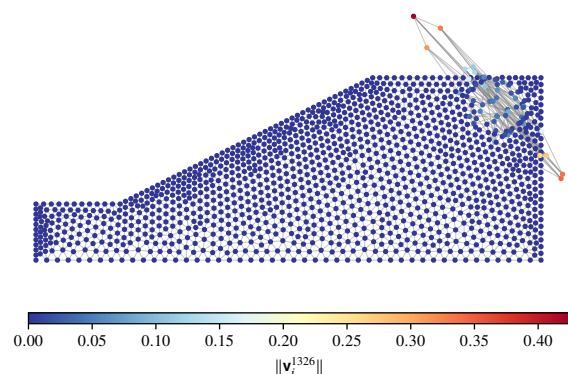
uses a coarser time grid based on a larger value for the minimum admissible load step in the adaptive load stepping algorithm used ($1 \cdot 10^{-2} \text{ s}$ instead of $1 \cdot 10^{-4} \text{ s}$),

$$\lambda^1 = 23.3449 \text{ Nm}^{-2}$$



(a) Eigenvector analysis corresponding to the second mode.

$$\lambda^{1326} = 18522826.7787 \text{ Nm}^{-2}$$



(b) Eigenvector analysis corresponding to a higher mode.

Figure 14 – Eigenvector analysis corresponding to higher modes of the last load step $t = 5.375 \text{ s}$. Plot over deformed configuration.

leading to earlier non-convergence of the simulation. Nevertheless, the simulation proceeded far enough to yield a comparable safety factor. The other variation (TRI6) uses triangular elements with quadratic shape functions and otherwise similar settings as TRI3a. The simulation with the higher-order elements reaches non-convergence much earlier and achieves a reduction of the smallest eigenvalue by only about three orders of magnitude compared to the nearly six orders of magnitude observed in the TRI3a simulation. However, the pole (vertical asymptote) of the curve and the extrapolation indicate that structural failure was achieved, as confirmed also by analysis of the displacement field. In

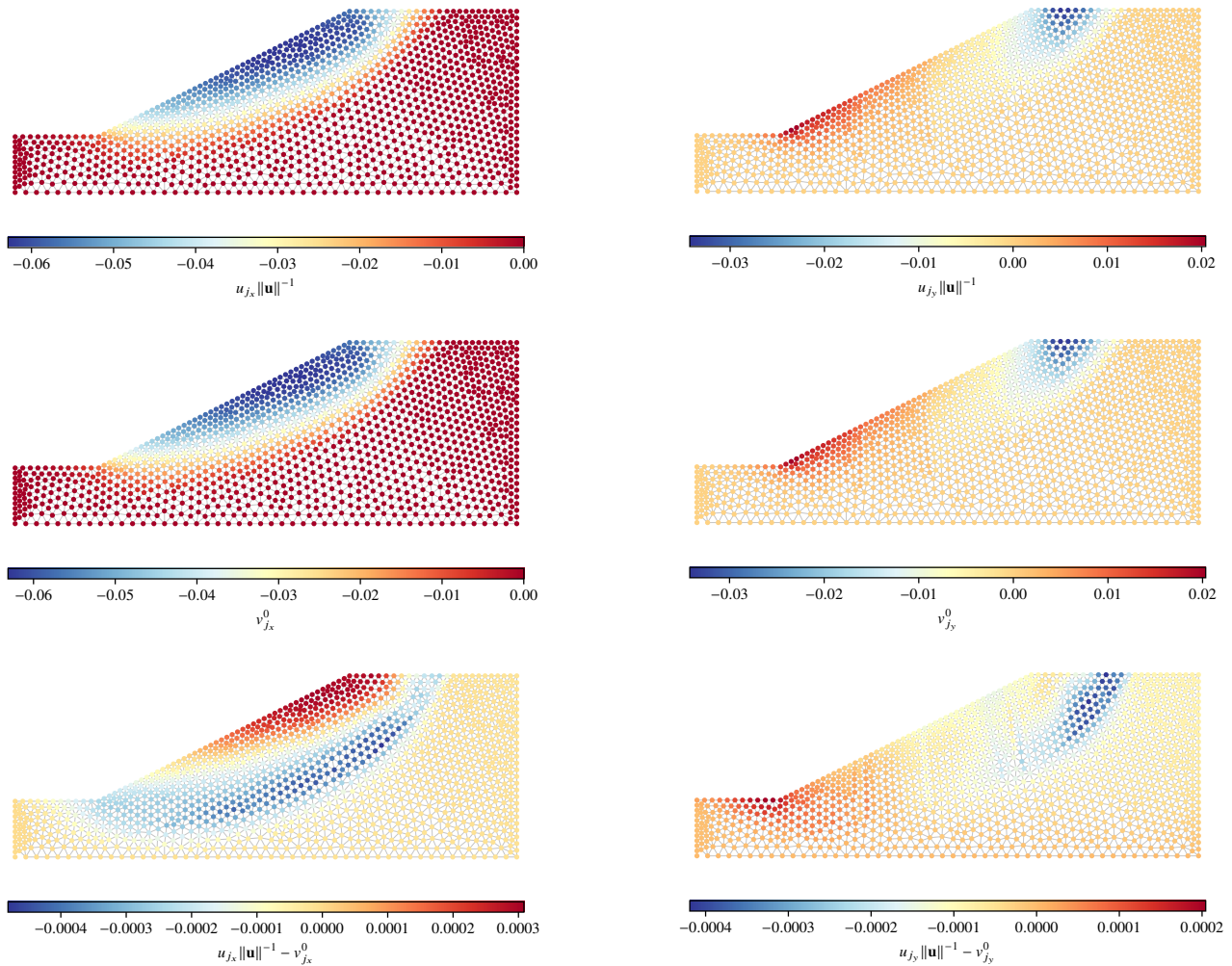


Figure 15 – Comparison of (normalized) displacement $\mathbf{u}/\|\mathbf{u}\|$ with the eigenvector \mathbf{v}^0 corresponding to the smallest eigenvalue. Top to bottom: normalized displacement vector, eigenvector corresponding to the smallest eigenvalue, difference of both. Left column shows horizontal component, right column vertical component. Plots over undeformed configuration. Note the change in scale between the two top rows and the bottom row, indicating the very small difference between the normalized displacement and the first eigenvector.

practice, such a sensitivity of the primary result to spatial discretization requires further analysis, e.g. by mesh convergence studies or regularization methods in case of strongly localizing problems.

Having studied the eigenvalues, we now look at the eigenvectors corresponding to the lowest eigenvalue (Figure 13). In the elastic case, Figure 13a, we observe a deformation mode with a characteristic length scale on the order of the structural length. After full load application, some plastification occurred and a pattern indicating a combination of ground bearing failure and slope failure starts to become visible to the trained eye in Figure 13b, such as slip circles in the slope and active earth pressure wedges under the top load. At the final load step, the eigenvector associated with the vanishing stiffness clearly looks like a slope failure problem, Figure 13c. We will investigate this particular vector more

closely later.

For completeness, we first look at some higher modes in the last load step in Figure 14. The eigenvector corresponding to the second smallest eigenvalue again delineates mainly the sliding soil mass, Figure 14a. Comparing Figures 13c and 14a, we see that the first and second modes show an increasing spatial frequency in relation to the structural length of the sliding part of the slope. This is analogous to what we saw in Section 3.2. Similarly, the eigenvectors corresponding to the highest eigenvalue show localized oscillations, modifying the solution at the corresponding position, cf. Figure 14b.

The eigenvector of the lowest eigenvalue can be analyzed in more detail in Figure 15. By means of Equation (15) we can speculate based on the results in Figure 11 that the eigenvector \mathbf{v}^0 should dominate the solution. In order to test this hypothesis, we normalize the

resulting displacement field (i.e. the full solution) and compare it to the zeroth eigenvector in Figure 15.

We find a strong visual resemblance in both the horizontal and lateral vector components, indicating that the principal deformation characteristics of the failing slope are captured by the eigenmode \mathbf{v}^0 . The difference between normalized displacements and the eigenmode is small compared to the values themselves. The main differences are concentrated around the shear band and the shoulder of the slope. These differences could in principle be reduced by including higher-order components as shown in Figure 9. This result opens up the avenue for reduced-order representations of the failure mode for this slope.

5 Discussion

In this article, illustrative examples for the analysis of global (structural) stiffness matrices were presented. As part of a special focus on structural failure, we investigated whether the eigenvector corresponding to the lowest eigenvalue of the stiffness matrix provides a useful estimator for the deformation mode during failure, even before reaching failure completely.

In the first example, eigenvalues and vectors were studied as a function of load in the case of a buckling rod. The eigenmodes showed clear relation to the buckling kinematics, and the lowest eigenvalue varied almost linearly with the load in this case, indicating that a linear extrapolation of the eigenvalues can be used to find zeros. In other words, the extrapolation of pre-failure information can be used to calculate the buckling load and estimate shapes.

The second example returned to a linear analysis of a rod under tension in a discrete finite element setting. The eigenvectors show a hierarchy of deformation contributions, each associated with an increasing stiffness and a shorter wave length. Vanishing eigenvalues were, in this linear setting, only associated with rigid body modes due to a lack of constraints. Sorting the eigenvalues and eigenvectors opened the way to model reduction, i.e. approximation of the full solution by fewer degrees of freedom relying on deformation characteristics. It could be seen that the approximation of the displacement using only the lowest eigenmode already gives a good approximation, particularly when the lowest eigenvalues are small in comparison to the remaining ones.

The third example is motivated by practical ultimate limit state analyses in geotechnical engineering. In this non-linear analysis, the eigendecomposition is performed on the global stiffness matrix⁷ of an elasto-plastic slope

⁷Note that this matrix is large in practical situations with size corre-

failure problem. For increasing strength reduction coefficients F_{trial} the lowest eigenvalue decreases and eventually approaches but does not reach zero. By extrapolation of the lowest eigenvalue evolution and by comparison of the associated eigenvector with the total displacement solution one can confirm the proximity to structural failure. We also showed the sensitivity of the result to numerical settings, a fact well-known from the literature. The eigenvector corresponding to the smallest eigenvalue gives a good approximation of the overall displacement results and again opens a path to model reduction.

6 Conclusions

This paper illustrated possible interpretations of eigenvalues and -vectors of global stiffness matrices. They provide instructive and unified ways of approaching material or structural failure, bifurcations, other singular points as well as certain types of model reduction. The relationship of (the lowest) eigenvalues with loads or material parameters can potentially be used to estimate critical points based on information from pre-critical states only. In non-linear problems this might, however, only be possible in the vicinity of the critical loads themselves, providing a limitation for the approach. Finally, visualizing the eigenvectors associated with the extremes of the eigenvalue distribution can help in finding causes for non-convergence in numerical simulations and thus be a helpful debugging tool.

Code Availability: The code behind the examples is provided in the form of Jupyter notebooks that can be found on GitHub⁸. The finite element code used in the strength reduction is available on GitLab⁹.

Acknowledgements: C. Hergl acknowledges the funding of the German Research Foundation (DFG) within the framework of the International Research Training Group on Computational Mechanics Techniques in High Dimensions GRK 2657 under Grant Number 433082294.

CRedit authorship contribution statement:

Ch. Hergl: writing – original draft, conceptualization, software, and visualization. *D. Kern:* writing – original draft, conceptualization, software, and visualization.

sponding to the number of degrees of freedom.

⁸<https://github.com/chiarMaHe/EigenmodeMinimalExample>. The precise version used for this publication is permanently stored at <https://archive.softwareheritage.org> with SWHID: `swh:1.dir:c2f9142d5b5f33a0f07925d3c44a3668e6ff5754`.

⁹<https://gitlab.opengeosys.org/ogs/ogs>

T. Nagel: writing – original draft, conceptualization, software, visualization, and supervision.

[19] J. Wauer. *Kontinuumsschwingungen*. Springer, 2014. ISBN 9783834818195.

References

- [1] AJ Abbo and SW Sloan. A smooth hyperbolic approximation to the mohr-coulomb yield criterion. *Computers & structures*, 54(3):427–441, 1995.
- [2] Z. Ambassa, J. C. Amba, and N. Tamaskovics. Implementation of the c-phi reduction procedure in cast3m code for calculating the stability of retaining walls in the layered backfill with strength parameters reduction by elasto-plastic finite element analysis using fields data. *Comptes Rendus. Mécanique*, 351:485–523, 12 2023. ISSN 1873-7234.
- [3] D. Bigoni. *Nonlinear Solid Mechanics: Bifurcation Theory and Material Instability*. Cambridge University Press, 2012. ISBN 9781139536981.
- [4] L. Bilke, B. Flemisch, T. Kalbacher, O. Kolditz, R. Helmig, and T. Nagel. Development of open-source porous media simulators: principles and experiences. *Transport in porous media*, 130:337–361, 2019.
- [5] J. Bleyer and G. Hassen. Automated formulation and resolution of limit analysis problems. *Computers & Structures*, 243:106341, 1 2021. ISSN 00457949.
- [6] T. Deng and T. Nagel. Slope failure analysis with strength reuction in opengeosys. 2021.
- [7] J. Guckenheimer and P. Holmes. *Nonlinear Oscillations, Dynamical Systems, and Bifurcations of Vector Fields*. Applied Mathematical Sciences. Springer New York, 2013. ISBN 9781461211402.
- [8] F. Hartmann and P. Jahn. *Statik und Einflussfunktionen – vom modernen Standpunkt aus*. Kassel University Press, 2016. ISBN 9783737601009.
- [9] L. Kafle, W.-J. Xu, S.-Y. Zeng, and T. Nagel. A numerical investigation of slope stability influenced by the combined effects of reservoir water level fluctuations and precipitation: A case study of the bianjiazhai landslide in china. *Engineering Geology*, 297:106508, 2 2022. ISSN 00137952.
- [10] Y.A. Kuznetsov. *Elements of Applied Bifurcation Theory*. Applied Mathematical Sciences. Springer New York, 2013. ISBN 9781475724219.
- [11] H. P. Langtangen and G. K. Pedersen. *Scaling of Differential Equations*. Simula SpringerBriefs on Computing. Springer International Publishing, 2016. ISBN 9783319327266.
- [12] Gentien Marois, Thomas Nagel, Dmitri Naumov, and Thomas Helfer. Invariant-based implementation of the mohr-coulomb elasto-plastic model in opengeosys using mfront, 2020.
- [13] N. C. Perkins and C. D. Mote Jr. Comments on curve veering in eigenvalue problems. *Journal of Sound and Vibration*, 106(3):451–463, 1986.
- [14] Plaxis2D. Phi-c reduction and comparison with bishop's method validation & verification. 2012.
- [15] Pedro M Reis. A perspective on the revival of structural (in) stability with novel opportunities for function: from buckliphobia to buckliphilia. *Journal of Applied Mechanics*, 82(11):111001, 2015.
- [16] F. Tschuchnigg, H.F. Schweiger, S.W. Sloan, A.V. Lyamin, and I. Raissakis. Comparison of finite-element limit analysis and strength reduction techniques. *Géotechnique*, 65:249–257, 4 2015. ISSN 0016-8505.
- [17] L.N. Virgin. *Vibration of Axially-Loaded Structures*. Cambridge University Press, 2012. ISBN 9781107406049.
- [18] LN Virgin and RB Davis. Vibration isolation using buckled struts. *Journal of Sound Vibration*, 260(5):965–973, 2003.